Wide-Angle Broadband Nonreflecting Acoustic Metamaterial Fence

Chenkai Liu,[1,2,‡] Chu Ma,[2,3,‡] Xinhao Li,[2] Jie Luo,[1] Nicholas X. Fang,[2,†] and Yun Lai[4,*]

[1] *School of Physical Science and Technology, Soochow University, Suzhou 215006, China*

[2] *Department of Mechanical Engineering, Massachusetts Institute of Technology, 77 Massachusetts Avenue, Cambridge, Massachusetts 02139, USA*

[3] *Department of Electrical and Computer Engineering, University of Wisconsin-Madison, Wisconsin 53706, USA*

[4] *MOE Key Laboratory of Modern Acoustics, National Laboratory of Solid State Microstructures, School of Physics, and Collaborative Innovation Center of Advanced Microstructures, Nanjing University, Nanjing 210093, China*

(Received 12 November 2019; revised manuscript received 13 February 2020; accepted 30 March 2020; published 6 May 2020)

In this work, we theoretically propose and experimentally demonstrate a kind of nonreflecting acoustic metamaterial fence that is perfectly impedance matched to air over a wide range of incident angles and a broad frequency band. The metamaterial fence is composed of an array of rigid cylinders with alternating layers of different cylinder diameters. It is designed by a spatially dispersive effective medium theory and experimentally demonstrated by airborne sound reflectance measurements. Our work provides a unique approach to design and realize rigid acoustic structures that can robustly prohibit reflection and reverberation. Such structures may have important applications in general acoustics.

DOI: 10.1103/PhysRevApplied.13.054012

I. INTRODUCTION

In the past decade, metamaterials have attracted great interest in the field of acoustics due to their unprecedented flexibility for manipulating acoustic waves [1–4]. With the development of synthetic acoustic materials with unusual mass density [5,6] and modulus [7–11], great progress has been made with numerous applications, which include negative refraction [12–14], cloaking [15–17], superresolution imaging [18–22], etc.

The property of impedance matching is crucial in the field of acoustic waves. Impedance mismatch leads to reflection and energy loss. In the design of an acoustic absorber [23], impedance matching is vitally important. While in some other acoustic devices and applications, it is also important to maximize the transmission as well as to reduce the reflection. Many ideals have been proposed to explore the possibility of maximizing transmission and minimizing reflection, such as Brewster's angle effect [24], antireflection coating [25], resonance enhancement [26–28], zero-index medium [29,30], complementary cancellation [31], topological effects [32–34], etc. These findings have extensively expanded the understanding of impedance-matching techniques, although most of them only work in a narrow frequency band or for a small range of incident angles.

Recently, an impedance-matching effect utilizing spatially dispersive parameters has been proposed for the realization of omnidirectional and broadband near-perfect transmission and zero reflection in electromagnetics and acoustics [35–41]. Such an approach has been shown to be very effective for designing metamaterials with omnidirectional and broadband impedance-matching properties.

In this work, we demonstrate that by applying the above approach, acoustic fences composed of arrays of rigid cylinders can be designed to be perfectly impedance matched to air over a wide angle range and a broad frequency band, and therefore exhibit the property of nonreflection, which is rather unusual for normal rigid structures in airborne acoustics [42,43]. Such a unique impedance-matching effect can be well explained by the spatially dispersive effective medium theory [35,38]. By fabricating samples using stereolithography 3D printing techniques, we experimentally verify this robust nonreflection property using sound reflectance measurements. We note here that the filling ratio of rigid cylinders is quite high at 0.37, and the working wavelength is comparable to the size of unit cells. Thus, such a phenomenon is a unique consequence of the eigenmode impedance-matching effect [35–40]. This work is an alternative experimental demonstration for such an impedance-matching effect in airborne sound waves. Our work proposes a systematic and efficient method to prohibit the general acoustic reflection and reverberation

*laiyun@nju.edu.cn

†nicfang@mit.edu

‡These authors contributed equally to this work.

from rigid fence structures. The method is quite general and could be applied to other rigid structures. Our work may find important applications in architectural and general acoustics.

II. ANALYTICAL DESIGN AND COMPUTATIONAL OPTIMIZATION

Consider a sound wave incident on a planar interface between an acoustic metamaterial (AMM) and the air background, shown in Fig. 1(a). The wave impedance of the air background can be defined as $Z_0 = \rho_0\omega/k_{0,x}$, where ρ_0, ω, and $k_{0,x}$ are the mass density, angular frequency, and x component of the wave vector in the air background, respectively. Assuming that the AMM can be described by an effective mass density tensor ρ_{eff} and an effective bulk modulus κ_{eff}, then the wave impedance of the AMM can be defined as $Z_{\text{eff}} = \rho_{\text{eff},x}\omega/k_x$, where $\rho_{\text{eff},x}$ and k_x are the x component of the effective mass density tensor of the AMM and wave vector in the AMM. If we can determine the appropriate parameters of the AMM to satisfy the impedance-matching condition $Z_{\text{eff}} = Z_0$ in a large range of angular frequencies and wave vectors, then the robust impedance-matching effect can be achieved [38].

A schematic illustration of the proposed acoustic metamaterial fence is shown in Fig. 1(a). The details of a unit cell are shown in Fig. 1(b), which comprises two types of rigid cylinders (A and B) with different diameters $D_A = 0.06a$ and $D_B = 0.08a$. Cylinders of each type are arranged in a square lattice. The unit cell is constructed in a symmetric way along the x direction, i.e., ABA structure. Parameters a and d are the lattice constant and the distance between neighboring cylinders ($d = 0.1a$), respectively.

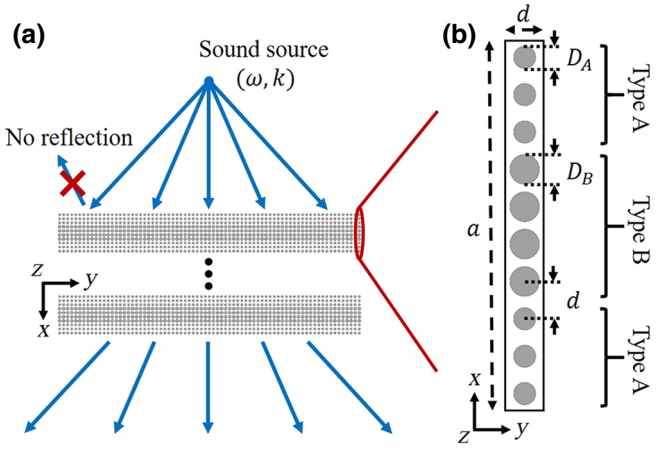

FIG. 1. (a) Schematic of the broadband and wide-angle nonreflecting acoustic metamaterial fence. The blue arrows represent sound waves radiated by a point source with angular frequency ω and wave vector k. (b) The unit cell composed of two types of rigid cylinders, type A and type B.

To obtain the acoustic performance of the designed metamaterial fence, we use the software COMSOL MULTIPHYSICS to conduct simulations. Figure 2(a) shows the band structure of the metamaterial fence and the red dashed line denotes the chosen normalized frequency $fa/c_0 = 0.76$, where f is the eigenfrequency and c_0 is the speed of sound in air. The equal frequency contours (EFCs) of the second band are shown in Fig. 2(b), and the particular EFC of $fa/c_0 = 0.76$ is shown as the red dashed line. It is seen that the EFC can be viewed as a part of an ellipse with a fitted function of $(k_x a/\pi - 1.51)^2/0.74 + (k_y a/\pi)^2 = 1.52^2$. Such a phenomenon has been proven in previous studies to support wide-angle impedance matching for electromagnetic waves and acoustic waves in water [35,37–40]. Figure 2(c) shows the impedance difference between the metamaterial fence and air $|(Z_{\text{eff}} - Z_0)/(Z_{\text{eff}} + Z_0)|$ at the second band regime. Blue color indicates good impedance matching, while red color indicates impedance mismatch. Clearly, we observe that the domain of impedance matching fills up a large portion in the Brillouin zone of the second band.

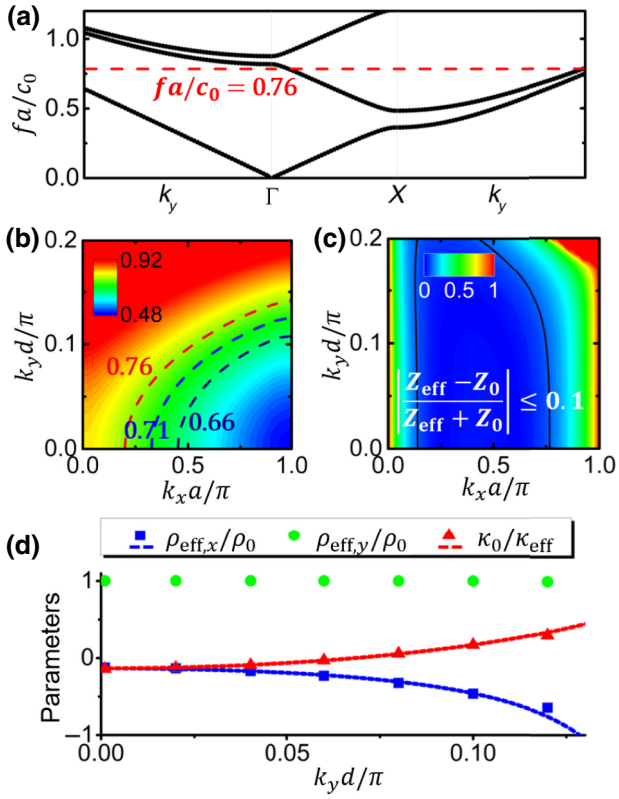

FIG. 2. (a) Band structure of the designed metamaterial fence. Red dashed line denotes the chosen normalized frequency of $fa/c_0 = 0.76$. (b) The EFCs of the second band. (c) The impedance difference between the fence and air $|(Z_{\text{eff}} - Z_0)/(Z_{\text{eff}} + Z_0)|$ at the second band regime. (d) Effective spatially dispersive parameters calculated from simulations (symbols) and analytical solutions (dotted lines) at $fa/c_0 = 0.76$.

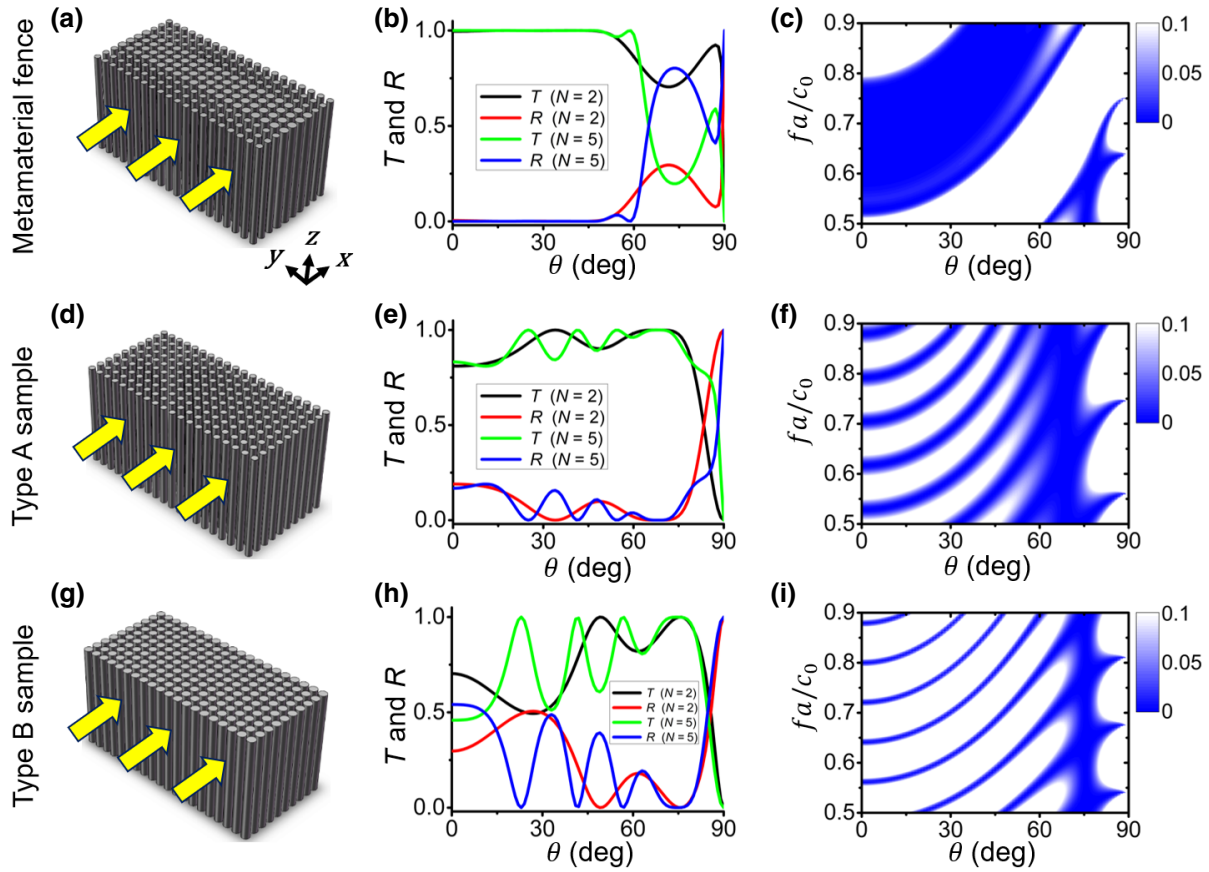

FIG. 3. Comparisons among the designed acoustic metamaterial fence, type A sample, and type B sample. (a) The numerical setup for the transmission and reflection computations for the acoustic metamaterial fence. (b) Incident-angle-dependent transmittance (T) and reflectance (R) for the metamaterial fence at $fa/c_0 = 0.76$. (c) Reflectance as functions of incident angles and frequencies for the metamaterial fence. Transmittance and reflectance for type A sample (d)–(f) and type B sample (g)–(i) for comparison.

Moreover, from Figs. 2(b) and 2(c), it is clearly seen that the impedance difference is quite small in the frequency range from 0.66 to 0.76, indicating a broadband and wide-angle impedance-matching effect. In addition, the effective parameters at $fa/c_0 = 0.76$ retrieved from the eigenfields method [38] are shown as symbols in Fig. 2(d). It is seen that both $\rho_{\text{eff},x}$ and κ_{eff} are dependent on k_y, indicating spatial dispersion. Here, due to weak modulation by periodic condition along the y direction, $\rho_{\text{eff},y}$ is almost equal to ρ_0. Moreover, by combining the impedance-matching condition and the shifted spatial dispersions, the analytical solutions of the AMM for perfect impedance matching can be described as

$$\rho_{\text{eff},x}/\rho_0 = -\left[1.51\pi/a - \sqrt{0.74(k_0^2 - k_y^2)}\right]/\sqrt{k_0^2 - k_y^2}$$

and

$$\kappa_0/\kappa_{\text{eff}} = \left\{k_y^2 - \left[1.51\pi/a - \sqrt{0.74(k_0^2 - k_y^2)}\right]\sqrt{k_0^2 - k_y^2}\right\}/k_0^2$$

respectively, and the results are shown as dotted lines in Fig. 2(d). The simulated results (symbols) coincide well with the analytical solutions (dotted lines), demonstrating the validity of the robust impedance-matching effect. The validity of the effective medium is discussed in detail in the Supplemental Material [44].

To verify the impedance-matching property, the reflectance and transmittance as functions of the incident angle and frequency are calculated with comsol simulations. We construct the metamaterial fence with unit cell array along the y direction and $N = (2, 5)$ unit cells along the x direction. The numerical setup for the propagation computation is shown in Fig. 3(a). The incident waves are marked as yellow arrows. For comparison, two contrasting samples, i.e., only type A sample and only type B sample, are also investigated, as shown in Figs. 3(d) and 3(g), respectively. Here, all cylinders in type A (B) sample are type A (B) cylinders. At the frequency $fa/c_0 = 0.76$, the simulated reflectance and transmittance as functions of incident angles and unit cell numbers ($N = 2, 5$) for the metamaterial fence, type A sample, and type B sample are shown in Figs. 3(b), 3(e), and 3(h), respectively. It is

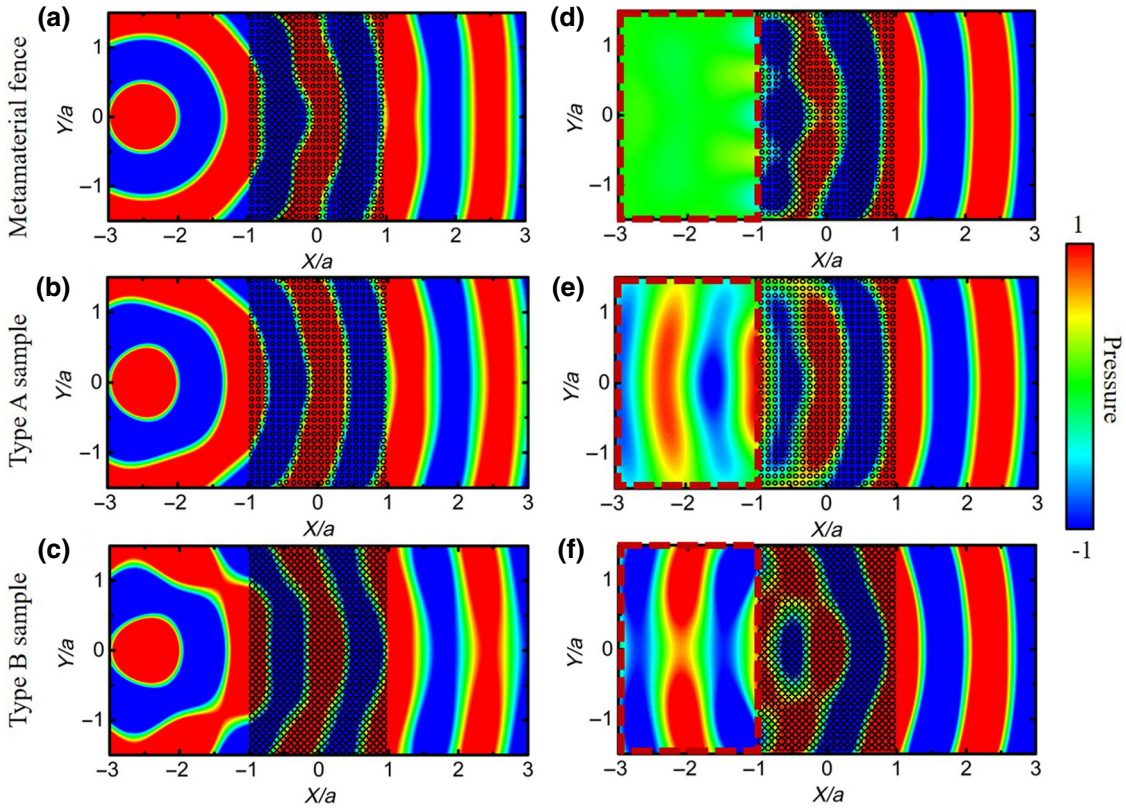

FIG. 4. Simulated pressure field distribution of the designed acoustic metamaterial fence, type A sample, and type B sample under a point source radiation at $fa/c_0 = 0.76$. (a)–(c) The total pressure field and (d)–(f) the scattered field.

seen that almost zero reflectance in a wide range of incident angles of $0^\circ \leq \theta \leq 60^\circ$ for sound waves propagating through the metamaterial fence is achieved and such a phenomenon is irrespective of the unit cell number N. Since loss is not considered here, transmission is almost unity. In contrast, the reflectance for type A sample and type B sample is generally nonzero and varies with the change of incident angles as well as the unit cell numbers. Moreover, we consider a broad frequency range of $fa/c_0 = 0.5$–0.9 to explore the broadband impedance-matching property. The simulated reflectance as functions of incident angles and frequencies for the metamaterial fence, type A sample, and type B sample is plotted in Figs. 3(c), 3(f), and 3(i), respectively. Here, the numbers of unit cells along the x direction are all set to $N = 5$. It is seen that type A sample and type B sample only have zero reflectance at particular discrete frequencies due to Fabry-Perot resonances, or at particular incident angles due to the Brewster effect. Notably, almost zero reflectance in a wide range of incident angles and a broad frequency band can be realized using the designed metamaterial fence. These results clearly demonstrate that the metamaterial fence exhibits the rare property of a robust impedance-matching effect. One example of the influence of perturbation is discussed in the Supplemental Material [44].

In order to further demonstrate the validity of the nonreflecting property, full-wave numerical simulations under a point source radiation located at $(X/a = -2.5, Y/a = 0)$ are performed. The frequency is chosen as $fa/c_0 = 0.76$. The designed metamaterial fence composed of $N = 2$ unit cells along the x direction is placed at $X/a \in [-1, 1]$. Also, we take the type A sample and type B sample into consideration for comparison. The total (scattered) acoustic pressure field distributions are shown in Figs. 4(a)–4(c) [Figs. 4(d)–4(f)]. Here, the scattered field is obtained by subtracting the free-space background field from the total field. Compared to the contrasting samples (type A and B samples), in which obvious reflection and reverberation occur [shown as red dotted box in Figs. 4(d), 4(e) and 4(f)] due to natural impedance mismatch, the designed metamaterial fence does not generate any reflection, demonstrating an almost perfect impedance-matching effect.

III. EXPERIMENTAL VERIFICATION

To experimentally verify the robust impedance-matching effect, we perform airborne sound reflectance measurements. As shown in Fig. 5(a), one sound speaker (used as a point source) and one microphone (used as a detector) are put inside a two-dimensional waveguide

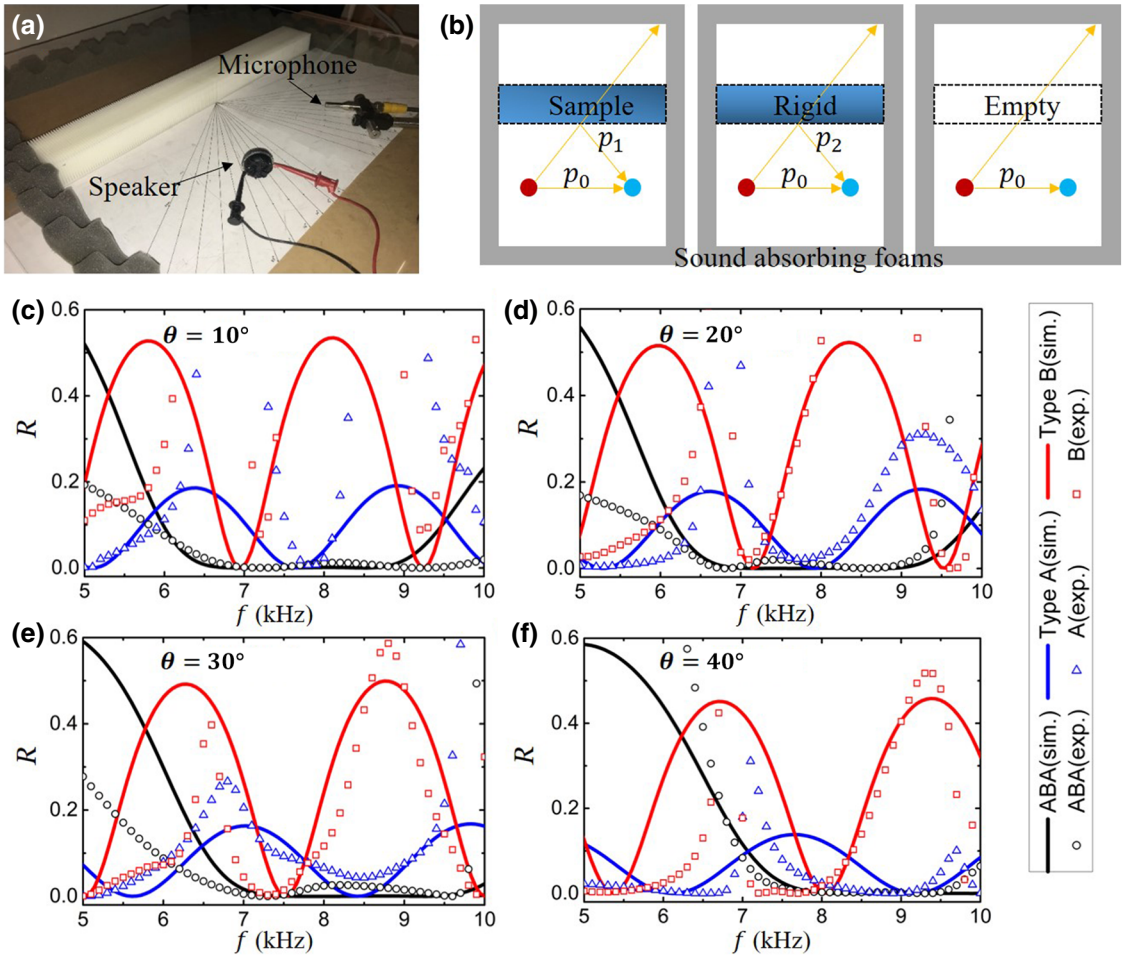

FIG. 5. Experiment of airborne sound reflectance measurements. (a) Photo of the experimental setup. (b) Schematic of the experimental procedures. (c)–(f) Comparisons of frequency-dependent reflectance for different incident angles through the metamaterial fence (ABA sample), type A sample, and type B sample. The symbols (solid lines) represent the experimental (simulated) results.

formed by two PMMA plates with a height of 30 mm. Sound-absorbing foams are put around the waveguide to eliminate the influence of unwanted reflection. The designed metamaterial fence, with a unit-cell size of $a = 30\,\text{mm}$, $d = 3\,\text{mm}$, and $N = 2$, is fabricated with resin using a stereolithography 3D printing method. The speaker emits a sound pulse containing waves in a frequency range of 5–10 kHz. By changing the position and orientation of the source, the incident angle varies in the range of 10°–40° (step size of 10°). When the incident angle changes, the position and orientation of the detector is also changed to the actual reflection angle, which is the same as the incident angle. We perform the following procedures to measure the reflectance for each incident angle, as shown in Fig. 5(b). Firstly, we measure the reflected signal from the metamaterial fence with desired incident and reflected angles, defined as $p_{\text{metamaterial}} = p_0 + p_1$, where p_0 and p_1 represent the directly arriving wave and the reflected wave, respectively. Then, a rigid sample is placed at the same position and the measured signal is defined as $p_{\text{rigid}} = p_0 + p_2$, where p_2 represents the reflected wave from the hard boundary. Finally, we measure the reflected signal from the free space (empty field), which is defined as $p_{\text{free space}} = p_0$. Therefore, the reflectance of the metamaterial fence under the desired incident angle can be defined as $R = |(p_{\text{metamaterial}} - p_{\text{free space}})/(p_{\text{rigid}} - p_{\text{free space}})|^2$. The measured reflectance as a function of frequency for different incident angles is shown in Figs. 5(c)–5(f). It is clearly seen that the contrasting samples (type A and type B) produce a frequency-dependent and incident-angle-dependent reflectance, with reflectance vanishing only at several discrete frequencies duo to Fabry-Perot resonance. On the other hand, the metamaterial fence exhibits near-zero reflectance in a wide range of incident angles and a broad frequency band. The measured results agree well with the simulation results. Therefore, the acoustic metamaterial fence demonstrates the rare property of a robust impedance-matching effect for such an array of rigid cylinders.

We note that, due to the acoustic dissipation, the measured transmittances are lower than those expected in the simulations. Nevertheless, when the dissipation is weak, the robust impedance-matching effect is still clearly observed in both simulations and measurements. Moreover, through adjusting the dissipation and geometry parameters, the unique phenomenon of broadband and wide-angle perfect absorption can be obtained. More details are shown in the Supplemental Material [44].

IV. CONCLUSION

In summary, we establish a kind of acoustic metamaterial fence that exhibits the rare property of robust impedance matching with air, and thus leads to zero reflection in a wide range of incident angles and a broad frequency band. The nonreflecting metamaterial fence, composed of two types of rigid cylinders with different diameters in an ABA arrangement, features an effective impedance that is perfectly matched with air. The unique phenomenon can be well explained by the spatially dispersive medium theory. The feasibility of the robust impedance-matching effect is verified in both full-wave simulations and experimental reflectance measurements. Our work demonstrates that delicate design of rigid structures can totally eliminate the reflection of sound. Such an unusual property may find applications in various fields of acoustics.

ACKNOWLEDGMENTS

Y.L. acknowledges financial support from the National Key R&D Program of China (2017YFA0303702), National Natural Science Foundation of China (61671314, 11974176), and a project funded by the Priority Academic Program Development of Jiangsu Higher Education Institutions (PAPD); C.M., X.L., and N.X.F. acknowledge support from Exxon Mobil through the MIT Energy Initiative.

[1] G. Ma and P. Sheng, Acoustic metamaterials: From local resonances to broad horizons, Sci. Adv. **2**, e1501595 (2016).
[2] S. A. Cummer, J. Christensen, and A. Alù, Controlling sound with acoustic metamaterials, Nat. Rev. Mater. **1**, 16001 (2016).
[3] H. Ge, M. Yang, C. Ma, M. H. Lu, Y. F. Chen, N. Fang, and P. Sheng, Breaking the barriers: Advances in acoustic functional materials, Natl. Sci. Rev. **5**, 159 (2018).
[4] B. Assouar, B. Liang, Y. Wu, Y. Li, J. C. Cheng, and Y. Jing, Acoustic metasurfaces, Nat. Rev. Mater. **3**, 460 (2018).
[5] Z. Liu, X. Zhang, Y. Mao, Y. Zhu, Z. Yang, C. T. Chan, and P. Sheng, Locally resonant sonic materials, Science **289**, 1734 (2000).
[6] Z. Yang, J. Mei, M. Yang, N. H. Chan, and P. Sheng, Membrane-type Acoustic Metamaterial with Negative Dynamic Mass, Phys. Rev. Lett. **101**, 204301 (2008).
[7] N. Fang, D. Xi, J. Xu, M. Ambati, W. Srituravanich, C. Sun, and X. Zhang, Ultrasonic metamaterials with negative modulus, Nat. Mater. **5**, 452 (2006).
[8] Y. Lai, Y. Wu, P. Sheng, and Z. Q. Zhang, Hybrid elastic solids, Nat. Mater. **10**, 620 (2011).
[9] Y. Wu, Y. Lai, and Z. Q. Zhang, Elastic Metamaterials with Simultaneously Negative Effective Shear Modulus and Mass Density, Phys. Rev. Lett. **107**, 105506 (2011).
[10] G. Ma, C. Fu, G. Wang, P. Del Hougne, J. Christensen, Y. Lai, and P. Sheng, Polarization bandgaps and fluid-like elasticity in fully solid elastic metamaterials, Nat. Commun. **7**, 13536 (2016).
[11] J. Shi, C. Liu, and Y. Lai, Controlling the effective bending stiffness via out-of-plane rotational resonances in elastic metamaterial thin plates, New J. Phys. **20**, 103043 (2018).
[12] T. Brunet, A. Merlin, B. Mascaro, K. Zimny, J. Leng, O. Poncelet, C. Aristégui, and O. Mondain-Monval, Soft 3D acoustic metamaterial with negative index, Nat. Mater. **14**, 384 (2015).
[13] Z. Liang and J. Li, Extreme Acoustic Metamaterial by Coiling up Space, Phys. Rev. Lett. **108**, 114301 (2012).
[14] S. Zhang, L. Yin, and N. Fang, Focusing Ultrasound with an Acoustic Metamaterial Network, Phys. Rev. Lett. **102**, 194301 (2009).
[15] S. A. Cummer and D. Schurig, One path to acoustic cloaking, New J. Phys. **9**, 45 (2007).
[16] H. Chen and C. T. Chan, Acoustic cloaking in three dimensions using acoustic metamaterials, Appl. Phys. Lett. **91**, 183518 (2007).
[17] S. Zhang, C. Xia, and N. Fang, Broadband Acoustic Cloak for Ultrasound Waves, Phys. Rev. Lett. **106**, 024301 (2011).
[18] N. Kaina, F. Lemoult, M. Fink, and G. Lerosey, Negative refractive index and acoustic superlens from multiple scattering in single negative metamaterials, Nature **525**, 77 (2015).
[19] J. Li, L. Fok, X. Yin, G. Bartal, and X. Zhang, Experimental demonstration of an acoustic magnifying hyperlens, Nat. Mater. **8**, 931 (2009).
[20] F. Lemoult, M. Fink, and G. Lerosey, Acoustic Resonators for far-Field Control of Sound on a Subwavelength Scale, Phys. Rev. Lett. **107**, 064301 (2011).
[21] C. Ma, S. Kim, and N. X. Fang, Far-field acoustic subwavelength imaging and edge detection based on spatial filtering and wave vector conversion, Nat. Commun. **10**, 204 (2019).
[22] G. Ma, X. Fan, F. Ma, J. De Rosny, P. Sheng, and M. Fink, Towards anti-causal green's function for three-dimensional sub-diffraction focusing, Nat. Phys. **14**, 608 (2018).
[23] M. Yang and P. Sheng, Sound absorption structures: From porous media to acoustic metamaterials, Annu. Rev. Mater. Res. **47**, 83 (2017).
[24] B. Manzanares-Martínez and F. Ramos-Mendieta, Transverse elastic waves in superlattices: The brewster acoustic angle, Phys. Rev. B **61**, 12877 (2000).
[25] H. K. Raut, V. A. Ganesh, A. S. Nair, and S. Ramakrishna, Anti-reflective coatings: A critical, in-depth review, Energy Environ. Sci. **4**, 3779 (2011).

[26] E. Bok, J. J. Park, H. Choi, C. K. Han, O. B. Wright, and S. H. Lee, Metasurface for Water-to-Air Sound Transmission, Phys. Rev. Lett. **120**, 44302 (2018).
[27] A. E. Miroshnichenko, S. Flach, and Y. S. Kivshar, Fano resonances in nanoscale structures, Rev. Mod. Phys. **82**, 2257 (2010).
[28] M. Landi, J. Zhao, W. E. Prather, Y. Wu, and L. Zhang, Acoustic Purcell Effect for Enhanced Emission, Phys. Rev. Lett. **120**, 114301 (2018).
[29] R. Fleury and A. Alù, Extraordinary Sound Transmission Through Density-Near-Zero Ultranarrow Channels, Phys. Rev. Lett. **111**, 055501 (2013).
[30] M. Dubois, C. Shi, X. Zhu, Y. Wang, and X. Zhang, Observation of acoustic dirac-like cone and double zero refractive index, Nat. Commun. **8**, 14871 (2017).
[31] C. Shen, J. Xu, N. X. Fang, and Y. Jing, Anisotropic Complementary Acoustic Metamaterial for Canceling out Aberrating Layers, Phys. Rev. X **4**, 041033 (2014).
[32] X. Zhang, M. Xiao, Y. Cheng, M.-H. Lu, and J. Christensen, Topological sound, Commun. Phys. **1**, 97 (2018).
[33] G. Ma, M. Xiao, and C. T. Chan, Topological phases in acoustic and mechanical systems, Nat. Rev. Phys. **1**, 281 (2019).
[34] H. He, C. Qiu, L. Ye, X. Cai, X. Fan, M. Ke, F. Zhang, and Z. Liu, Topological negative refraction of surface acoustic waves in a weyl phononic crystal, Nature **560**, 61 (2018).
[35] J. Luo, Y. Yang, Z. Yao, W. Lu, B. Hou, Z. H. Hang, C. T. Chan, and Y. Lai, Ultratransparent Media and Transformation Optics with Shifted Spatial Dispersions, Phys. Rev. Lett. **117**, 223901 (2016).
[36] K. Im, J. H. Kang, and Q. H. Park, Universal impedance matching and the perfect transmission of white light, Nat. Photonics **12**, 143 (2018).
[37] Z. Yao, J. Luo, and Y. Lai, Photonic crystals with broadband, wide-angle, and polarization-insensitive transparency, Opt. Lett. **41**, 5106 (2016).
[38] C. Liu, J. Luo, and Y. Lai, Acoustic metamaterials with broadband and wide-angle impedance matching, Phys. Rev. Mater. **2**, 045201 (2018).
[39] Z. Yao, J. Luo, and Y. Lai, Illusion optics via one-dimensional ultratransparent photonic crystals with shifted spatial dispersions, Opt. Express **25**, 30931 (2017).
[40] J. Luo and Y. Lai, Near-perfect absorption by photonic crystals with a broadband and omnidirectional impedance-matching property, Opt. Express **27**, 15800 (2019).
[41] M. Zheng, X. Liu, Y. Chen, H. Miao, R. Zhu, and G. Hu, Theory and Realization of Nonresonant Anisotropic Singly Polarized Solids Carrying Only Shear Waves, Phys. Rev. Appl. **12**, 014027 (2019).
[42] F. Cervera, L. Sanchis, J. V. Sánchez-Pérez, R. Martínez-Sala, C. Rubio, F. Meseguer, C. López, D. Caballero, and J. Sánchez-Dehesa, Refractive Acoustic Devices for Airborne Sound, Phys. Rev. Lett. **88**, 023902 (2002).
[43] D. Torrent, A. Håkansson, F. Cervera, and J. Sánchez-Dehesa, Homogenization of two-Dimensional Clusters of Rigid Rods in air, Phys. Rev. Lett. **96**, 204302 (2006).
[44] See Supplemental Material at http://link.aps.org/supplemental/10.1103/PhysRevApplied.13.054012 for more detailed discussions for validity of the effective medium, perturbation, and dissipation.